

Learning Super-resolved Depth from Active Gated Imaging

Tobias Gruber^{1,2}, Mariia Kokhova^{1,3}, Werner Ritter¹, Norbert Haala³ and Klaus Dietmayer²

Abstract—Environment perception for autonomous driving is doomed by the trade-off between range-accuracy and resolution: current sensors that deliver very precise depth information are usually restricted to low resolution because of technology or cost limitations. In this work, we exploit depth information from an active gated imaging system based on cost-sensitive diode and CMOS technology. Learning a mapping between pixel intensities of three gated slices and depth produces a super-resolved depth map image with respectable relative accuracy of 5% in between 25–80 m. By design, depth information is perfectly aligned with pixel intensity values.

I. INTRODUCTION

Safe autonomous driving at level five requires perfect environment perception under any conditions, even in bad weather. Active gated imaging is a promising technology that improves vision especially in bad weather as it removes backscatter by time-synchronizing illumination and exposure. It was shown in an image sensor benchmark [1] that active gated imaging outperforms standard imaging in foggy conditions. In addition to stable contrast in most weather conditions, active gated imaging can provide depth information by suitable post-processing. Several approaches exist for accessing this depth information. However, these approaches are mostly restricted to certain laser pulse forms and delays. In this work, we describe an approach to estimate depth for a completely free-shaped range intensity profile (RIP) based on neural networks (NNs). As depicted in Fig. 1, we use three overlapping slices in order to obtain a depth map. Range is estimated pixel-wise by finding a nonlinear function that maps the three intensity values of the slices to a range. We use the combination of a gated camera system and a light detecting and ranging (lidar) sensor in order to obtain labeled data by simply driving in a natural environment. It is shown that a very simple single hidden layer neural network with 40 nodes is able to estimate range with approximately 5% relative accuracy for a distance range in between 25–80 m. Our depth estimation can be described as super-resolved since the gated camera has a resolution of 1280x720 pixels.

¹ The authors are with Daimler AG, RD/AFU, Wilhelm-Runge-Str. 11, 89081 Ulm, Germany, tobias.gruber@daimler.com, mariia.kokhova@daimler.com, werner.r.ritter@daimler.com

² The authors are with the Institute of Measurement, Control and Microtechnology, Ulm University, Albert-Einstein-Allee 41, 89081 Ulm, Germany klaus.dietmayer@uni-ulm.de

³ The authors are with the Institute for Photogrammetry, University of Stuttgart, Geschwister-Scholl-Str. 24D, 70174 Stuttgart, Germany norbert.haala@ifp.uni-stuttgart.de

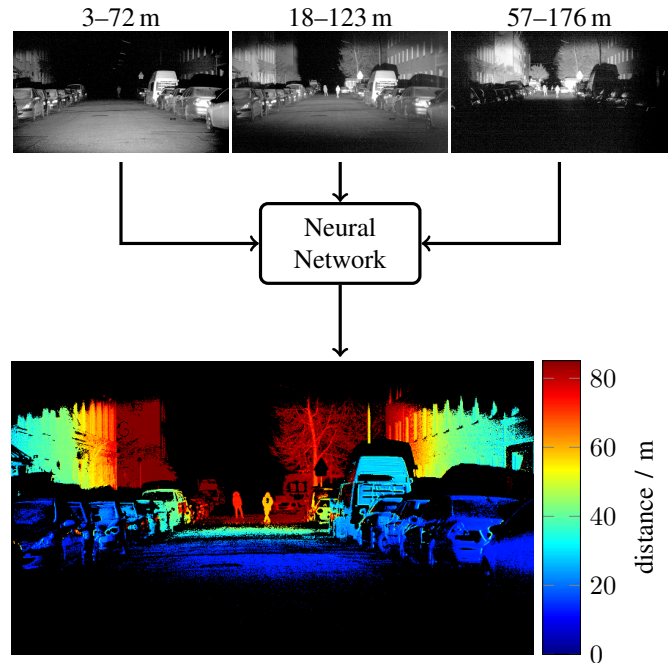


Fig. 1: A neural network (NN) processes three slices of an active gated imaging system and yields a depth map.

A. Related Work

1) *Active Gated Imaging*: First successful feasibility tests for active gated imaging were first reported in 1967 by Heckmann and Hodgson [2]. The purpose of this technique was to improve efficiency of underwater photography by avoiding backscattering. Their system consisted of a light source that emitted short high-intensity bursts of light and a receiver that could be opened and closed very fast. Further development of this technology was driven mainly by military research and led to many applications such as target identification [3], night vision [4], underwater imaging [5] and three-dimensional imaging [6]. In comparison to laser scanning, the result of active gated imaging is a two-dimensional image of the scene. However, by capturing multiple gated images with different delays, it is also possible to obtain range information. The first approach to estimate distance was done in order to identify sea mines on the seabed [6]. By using cost sensitive components such as laser diodes and a complementary metal-oxide semiconductor (CMOS) imager, Brightway Vision wants to establish such a gated system for use as a night vision system on the automotive market [4]. In this work, such a system is extended with three-dimensional imaging and evolves into a *range camera*.

2) *Time Slicing Method*: First attempts to extract depth from multiple gated images were made at the beginning of the century especially driven by defense research. Busck and Heiselberg [6] introduced the *time-slicing method* for range estimation which samples the gate delay profile (GDP) temporally with a single target by increasing the delay in steps and estimates the range by a weighted average [7]. Similar work has been done by He and Seet [8] where they sampled the GDP spatially with multiple targets at certain distances. Andersson presented in [9] two other depth reconstruction methods based on a sampled GDP: least-squares parameter fitting and data feature positioning. In recent years, Chua et al. developed a noise-weighted average range calculation in order to handle noise influence better [10]. However, sampling the GDP requires recording many images of the same scene. This is no problem if the scene is stationary, but not suitable for real-time depth estimation in changing scenes.

3) *Range-intensity Correlation Method*: Depth accuracy of the time slicing method strongly depends on a huge number of very short pulse widths and scanning step sizes [6], [7], [9]. The work of Laurenzis et al. [11] tries to overcome this resolution limit by exploiting the trapezoidal shape of the RIP. This *range-intensity correlation method* requires a series of images with overlapping RIPs. In the overlapping region of a plateau and a rising or falling ramp, one can estimate the pixel-wise distance according to the relation of the intensities in both images by linear interpolation. They improved the previous method for non-trapezoidal RIPs and find a transformation rule from intensities to estimated distance by fitting a multi-order ratio-polynomial model [12]. The linear interpolation method for trapezoidal shapes was generalized to triangular shaped RIPs in [13]. For all of these range-intensity correlation methods perfect prior knowledge of the RIPs is required. Due to imperfections at laser pulse and gate shape modeling, e.g. rise and fall times, this is often very hard to obtain. Moreover, methods in [11], [12], [13] are limited to a rectangular modeling of the laser pulse and gate shape.

4) *Gain Modulation Method*: The gain modulation method, introduced in 2008 by Xiuda et al. [14], is a method independent from the laser pulse shapes. However, for this method it is important that the laser pulse width is much smaller than the gate duration. By using a gain-modulated and a gain-constant image, it is possible to recover depth. The modulation can be linear [14] or exponential [15].

5) *Recent Range Reconstruction Methods*: In recent years, correlated double sampling was developed [16] that is able of capturing two images with different delays from a single laser pulse. This hardware adaption makes range reconstruction methods faster. Due to the rising interest in convolutional neural networks (CNNs), there is also a lot of movement in the area of depth map prediction from a single image, e.g. [17]. However, these methods are not comparable to our approach as they either use special hardware or RGB images.

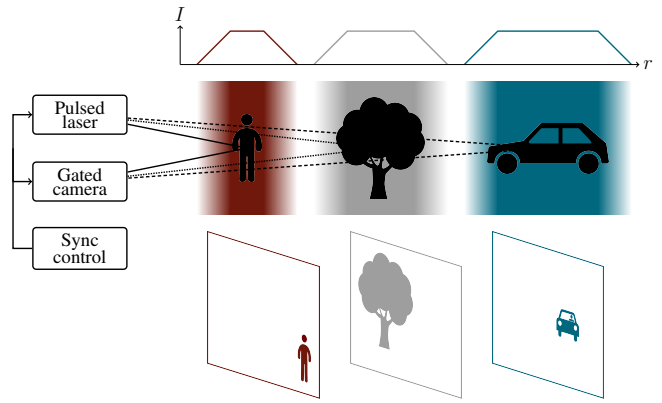


Fig. 2: Description of the active gated imaging system.

II. GETTING DEPTH FROM GATED IMAGES

Active gated imaging is based upon a sensitive image sensor and its own illumination source as depicted in Fig. 2. By time-synchronizing the image sensor and its illumination, it is possible to capture an image at a certain range, referred to as *slice* in the following. The scene is illuminated with a very short laser pulse and the camera gate opens after a designated delay t_0 in order to receive only photons from a certain distance r . This helps to select the reflected light from objects and block back-scattered photons from clouds, fog or raindrops. In order to improve the signal-to-noise-ratio (SNR) on the imager, multiple number of pulses are usually collected on the chip [6]. Active gated imaging delivers images with high contrast even in extreme scattering conditions as in fog or underwater. However, active illumination means dealing with eye-safety restrictions and interference with similar systems.

For the sake of simplicity, suppose that the shape of the laser pulse $p(t - 2r/c_0)$ and the detector gain $g(t - t_0)$ are rectangular with length t_L and t_G respectively (see Fig. 3a and 3b), where c_0 denotes the speed of light. Following [9], the pixel value $I(t_0, r)$ is proportional to the convolution of p and g , thus

$$I(t_0, r) \propto \int_{-\infty}^{\infty} g(t - t_0) p\left(t - \frac{2r}{c_0}\right) dt. \quad (1)$$

A. Gate Delay Profile (GDP)

The GDP $I_{\text{GDP}}(t_0)$ describes the pixel intensity of an object at a certain distance r if the delay t_0 is varied. If $t_L = t_G$ the shape of $I_{\text{GDP}}(t_0)$ is triangular, otherwise trapezoidal (see Fig. 3c). As introduced in [7], depth can be estimated from the GDP by *time-slicing*, that means sampling the GDP by increasing the camera delay t_0 in n steps with $\Delta t \ll t_L, t_G$ and estimate the depth by a conventional weighted average method. The average two-way travel time

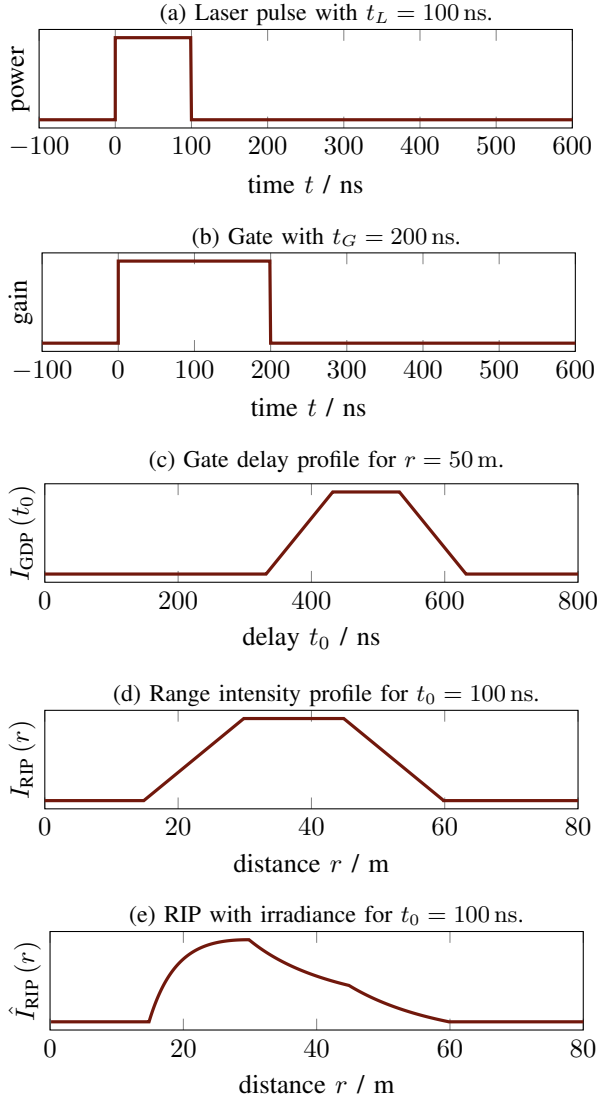


Fig. 3: Example simulation of gate delay profile (GDP) and range intensity profile (RIP). Y-axis can be arbitrary scaled.

\hat{t} is obtained by

$$\hat{t} = \frac{\sum_{i=1}^n I_i t_i}{\sum_{i=1}^n I_i} \quad (2)$$

where I_i is the pixel intensity and $t_i = t_0 + i\Delta t$ the delay of slice i . and the depth of the pixel \hat{r}_{ts} can be reconstructed by

$$\hat{r}_{ts} = \frac{c_0 \hat{t}}{2}. \quad (3)$$

However, the time-slicing method assumes a Gaussian laser pulse shape. Literature shows that usually 10 to 100 slices are used for sampling a small range at close distance, resulting in an accuracy of 1 mm [6], [7], [9]. Increasing the range of depth estimation would require many more slices or else result in lower accuracy. Therefore, high accuracy and large depth of field cannot be realized simultaneously.

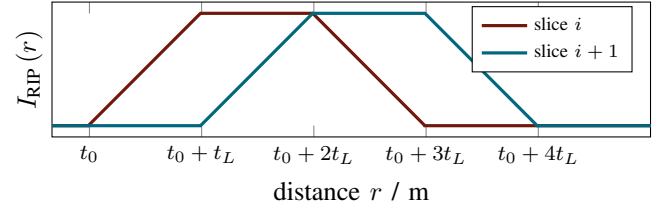


Fig. 4: Example range intensity profiles (RIPs) for two similar slices with $t_G = 2t_L$.

B. Range Intensity Profile (RIP)

In contrast to the GDP, the RIP $I_{RIP}(r)$ characterizes the pixel intensity for a fixed slice with delay t_0 with respect to distance r . Similar to the GDP, the shape of the RIP is basically trapezoidal for $t_L \neq t_G$, see Fig. 3d. However, the pixel value of the RIP additionally depends on the laser pulse irradiance $J(r)$, the reflectance α of the target i and the influence of the atmosphere $\beta(r)$. Therefore, one can write $I_{RIP}(r)$ as

$$\hat{I}_{RIP}(r) \propto \kappa(r) \int_{-\infty}^{\infty} g(t - t_0) p\left(t - \frac{2r}{c_0}\right) dt \quad (4)$$

where $\kappa(r)$ is a distance dependent factor given by

$$\kappa(r) = J(r) \alpha \beta(r) = \frac{1}{r^2} \alpha \beta(r). \quad (5)$$

An example for $I_{RIP}(r)$ is given in Fig. 3e.

The idea of *range-intensity correlation* is to exploit the spatial correlation of overlapped gated images. For an object at a certain distance r_0 the factor $\kappa(r_0)$ is constant and can be removed by considering only the intensity ratios.

Suppose that for two slices i and $i+1$ with gate duration $t_G = 2t_L$ and delay $t_i = t_0$ and $t_{i+1} = t_0 + t_L$, then $I_i(r)$ and $I_{i+1}(r)$ are trapezoidal and overlapping, see Fig. 4. According to [11], depth information for distance where slice i is a plateau and slice $i+1$ is rising, depth can be reconstructed by

$$\hat{r}_{\text{corr, trapez}} = \frac{c_0}{2} \left(t_0 + t_L + \frac{I_i}{I_{i+1}} t_L \right). \quad (6)$$

For triangular pulse shapes, a plateau is defined by $I_i + I_{i+1}$ and depth for distances where both slices are rising is estimated by

$$\hat{r}_{\text{corr, triangle}} = \frac{c_0}{2} \left(t_0 + t_L + \frac{I_i}{I_i + I_{i+1}} t_L \right). \quad (7)$$

These equations can be adapted to any region where two RIPs overlap.

This method works especially well for gated images with special pulse shapes, i.e. trapezoidal [11] or triangular [13], and adapted delays to generate these overlapping regions. For a depth scene of 650–1250 m, an accuracy of about 30 m was achieved in [12].

In order to get rid of the assumption of rectangular pulses, the *gain modulation method* was proposed in [14] and [15]. Two gated images are required for this method, i.e. a gain

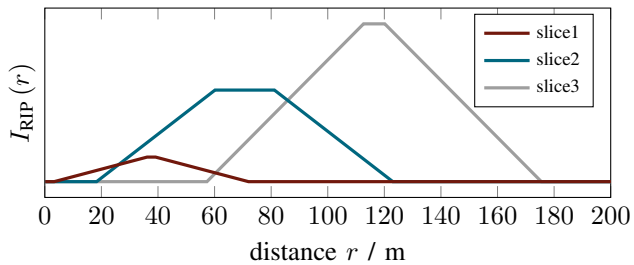


Fig. 5: Range intensity profiles (RIPs) of our gated parameters as described in Table I.

TABLE I: Gating parameters.

	slice1	slice2	slice3
pulses	202	591	770
t_L / ns	240	280	370
t_G / ns	220	420	420
t_0 / ns	20	120	380

modulated image and a gain constant image. Depth can then be estimated, similar to range-intensity correlation, by the relation of both intensities. In [14], depth accuracies around 1 m are achieved for a range from 800–1100 m. However, this method requires special imagers that are capable of providing modulated gain.

C. Why are these approaches not suitable?

While time slicing is more appropriate for high accuracy and small ranges, range-intensity correlation and gain modulation have benefits for larger ranges at the expense of lower accuracy. Gain modulation requires only two slices whereas range-intensity correlation requires more slices for long ranges and high accuracy. All methods prescribe conditions on certain pulse shapes, gate shapes and delays.

The idea of active gated imaging allows adapting the gating parameters so that the image offers maximal contrast at every distance. For example, for larger distances longer exposure times helps to capture more photons. Moreover, additional laser pulses at greater distances improve the SNR. If gating parameters are set up in order to improve the image quality, then current approaches have problems because their requirements are not satisfied anymore.

This work focuses on the automotive application of depth estimation from gated images. Hence, we apply the gating parameters as provided in Table I, resulting in three RIPs as depicted in Fig. 5. In order to allow these flexible gated settings which can adapt to the appearance of the scene, new ideas have to be found for recovering depth from slices. In the following chapter, we propose a method to estimate depth for free-modeled gated profiles without any restrictions.

D. Baseline Approach

As a baseline our approach has to compete with, we implemented a range-intensity correlation algorithm for our special gating parameters: the distance range is divided into 9 sections where the behavior of the slices differ (rising, plateau, falling) and range is estimated according to Equations 6 and 7. If distance can be estimated in two ways, e.g. in

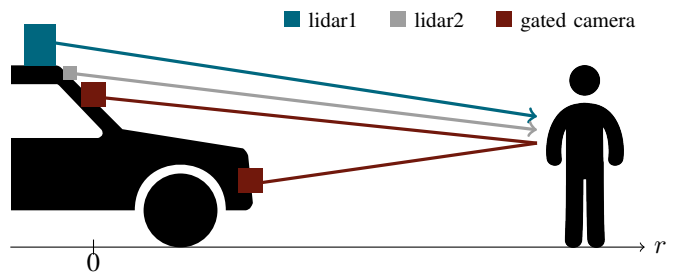


Fig. 6: Sensor setup: lidar1 - Velodyne HDL64 S3, lidar2 - Velodyne VLP32C, gated camera system - Brightway Vision.

between 57–72 m as depicted in Fig. 5, the distance estimate is given by the mean. This approach is a first attempt to make our approach comparable to other range-intensity correlation algorithms.

III. NEURAL NETWORK GATED DEPTH ESTIMATION

As described by Sonn et al. in [18], the problem of estimating depth from intensity values of different slices is basically a problem of estimating a function f that maps these intensity values to depth. In [12], a simple 5th order ratio-polynomial model was used to approximate depth from a pixel relation value. In this work, we describe a method to learn such a function with a simple neural network (NN).

Following [19], a multilayer NN with nonlinear activation functions can theoretically approximate any continuous function on a bounded region arbitrarily closely—if the number of neurons is large enough. A NN defines an input-output mapping $f(x; \theta)$ by a chain of functions, thus,

$$y = f(x; \theta) = f^{(L-1)} \left(f^{(L-2)} \left(\dots \left(f^{(0)}(x) \right) \right) \right) \quad (8)$$

where x , y , θ and L denote input, output, parameters and depth respectively.

Each function $f^{(l)}$ describes a layer that consists of many neurons. For every neuron, all of its weighted inputs are added up, a bias is optionally added, and the result is propagated through a nonlinear activation function, e.g., a sigmoid, hyperbolic tangent or a rectified linear unit (ReLU).

By using a training set of known input-output mappings, the optimal parameters θ can be found that approximate f best. Training is done by minimizing a loss function with gradient descent optimization methods and the backpropagation algorithm [20]. For a more detailed description of the theory of deep learning, we refer the interested reader to [21].

A. Collection of Training Data

Data for training the NN were recorded by a test vehicle equipped with two light detecting and ranging (lidar) systems (Velodyne HDL64 S3D and Velodyne VLP32C) and a gated imaging system from Brightway Vision, see Fig. 6. The gated camera offers 8 bit images with a resolution of 1280x720 pixels released at a frame rate of 120 Hz. The Velodyne lidar systems offer a distance accuracy of < 2 cm and a range of 120 m for objects with 80% reflectance. Intrinsic

and extrinsic calibration was performed in order to project lidar points into the rectified gated image. The different mounting positions of laser illumination and camera can be compensated by setting an additional delay offset.

For the current sensor setup, recording at night is much easier because no additional illumination of the sun has to be considered. Nevertheless, active gated imaging at day is not a problem if the laser power is high enough: subtracting a passive image from an active illuminated image yields the typical gated images. In order to focus on the algorithm and to make things easier, the dataset was recorded at night in Hamburg and Copenhagen. In total, we recorded approximately 2 million samples where each consists of three pixel intensities from each slice and its corresponding distance from the lidar point cloud. Since light propagates on the surface of a sphere, we consider the geometric distance $r = \sqrt{x^2 + y^2 + z^2}$ as reference.

We propose to train a NN for depth estimation with intensities of three slices as input and distance from our reference system as output. Nevertheless, some preprocessing of our dataset is required before.

B. Dataset Preprocessing

1) *Prefiltering*: The raw dataset includes points that are not illuminated or saturated. These points do not carry any representative information for the depth reconstruction and have to be filtered out. *Saturated points* can appear on the image because of the very high reflectance of some objects, e.g. traffic signs. All points with the gray pixel values greater than 250 are filtered out and are not used for the further training and evaluation. *Unilluminated points* are the pixels that do not register any reflected photons back. Usually, unilluminated pixels appear in the sky and in the border areas of the camera. All samples with a difference between maximum and minimum intensity that is less than 6 are also filtered out.

2) *Filtering*: Analysis of the training data shows that points exist with the same intensity triples but different distances. This can be explained by shadowing effects due to different mounting positions of the sensors on the car, projection error due to moving objects and rotating lidars, calibration error and lidar measurement noise. In order to improve the quality of our training data, different filtering algorithms are applied.

Our dataset consists of intensity triples and its corresponding distance. Intensity triples usually appear multiple times with slightly different distances or sometimes in case of errors with completely different distances. Filtering is based on the mean range for each intensity triple contained in the dataset. For *dataset1* and *dataset2*, we filter out all samples whose range differs more than 1 m from the mean range and less than 3 range occurrences. Afterwards, the mean is recalculated. While *dataset1* consists only of the recalculated mean value, *dataset2* includes all filtered samples that may describe the distributions better.

Fig. 7 depicts the distribution of the dataset samples. For distances larger than 60 m, there exists only a small amount

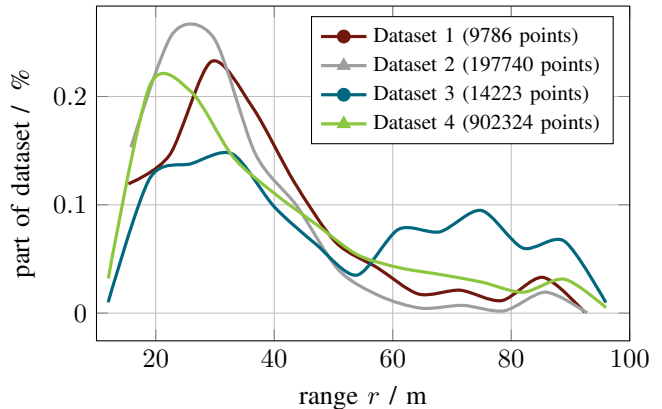


Fig. 7: Number of points in each dataset with respect to distance.

TABLE II: Grid search parameters.

Hyper parameters	Values
Learning rate	0.1, 0.01, 0.001
Batch size	4, 8, 16, 32, 64, 128, 256, 512
Network architecture	5, 10, 20, 40, 10-5, 20-10, 40-20, 20-10-5, 40-20-10, 40-20-10-5
Activation function	tanh, sigmoid, ReLU

of training samples. Therefore, for *dataset3*, we soften the filter criteria for distances larger than 60 m as follows: samples are filtered out if range differs more than 2 m and no minimum number of range occurrences is required.

dataset4 is the unfiltered dataset and includes all collected points. It contains a lot of noise and outliers. We will investigate how good the network can deal with these disturbances.

3) *Standardization*: In order to make the input values invariant to reflectance and ambient illumination, every sample $S_i = (s_{i1}, s_{i2}, s_{i3})$ is standardized by

$$\bar{S}_i = \frac{S_i - \mu_i}{\sigma_i} \quad (9)$$

where $\mu_i = \frac{1}{3} \sum_{j=1}^3 s_{ij}$ and $\sigma_i = \sqrt{\frac{1}{3-1} \sum_{j=1}^3 |s_{ij} - \mu_i|^2}$.

C. Network Design

As there is not yet a standard network for our task, an appropriate network design has to be found. The main focus of this work is to present the basic idea and not to find the perfect architecture and structure. Therefore, we do not spend too much effort and perform just a simple grid search over different network sizes and activation functions. Grid search means iterating over a finite set of different parameter combinations. Table II shows the parameter of the grid search. We introduce the notation 20-10-5 which describes the architecture of a NN employing three hidden layers with 20, 10 and 5 nodes, respectively.

As a loss function, we choose the mean absolute error (MAE). Weights and biases are initialized random uniformly between ± 0.05 and zeros respectively. We train our network

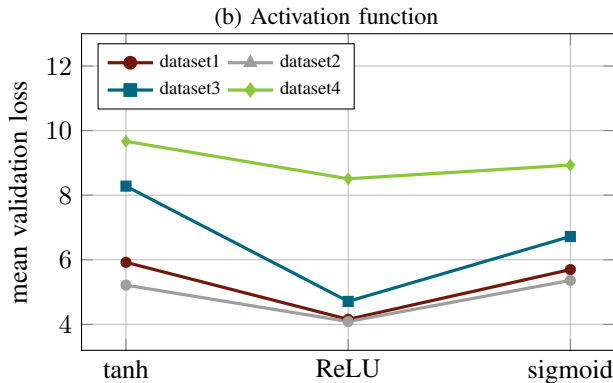
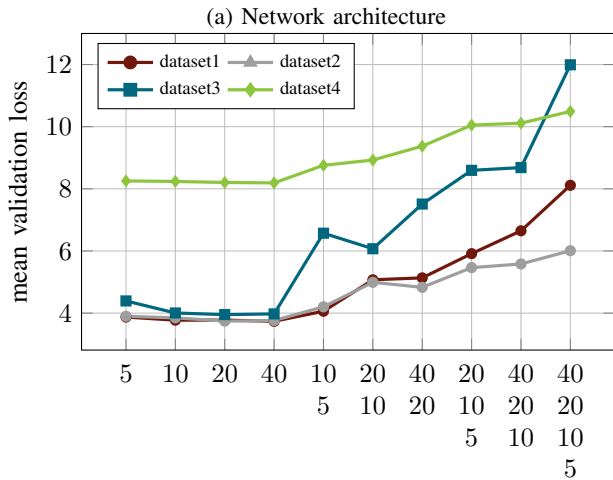


Fig. 8: Results of grid search.

TABLE III: Training parameters for each dataset.

	learning rate	batch size
dataset1	0.1	64
dataset2	0.01	32
dataset3	0.01	16
dataset4	0.01	256

for a maximum number of 100 epochs incorporating an early stopping condition.

In order to assess the grid search, the dataset has to be split into a training set and a validation set. In our case, we choose 80% for training and 20% for validation. A test set is recorded separately as explained in the next section.

Two main results of the grid search for hyper parameter optimization are shown in Fig. 8. In order to make the results of different datasets comparable, we search for a single network that performs best for all datasets and not for the best network for each dataset individually. Fig. 8a shows the mean validation loss for different network architectures. For each dataset, a simple NN with a single hidden layer with 40 nodes seems to be best for our task. According to Fig. 8b, the ReLU activation function in general performs best. In the following evaluation, we use a single hidden layer NN with 40 nodes and a ReLU activation function. Training parameters such as learning rate and batch size are adapted individually for each dataset, see Table III.

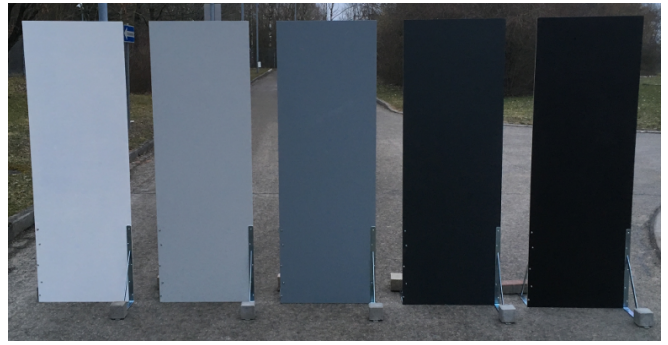


Fig. 9: Targets for test set. From left to right: white, light gray, middle gray, dark gray, black.

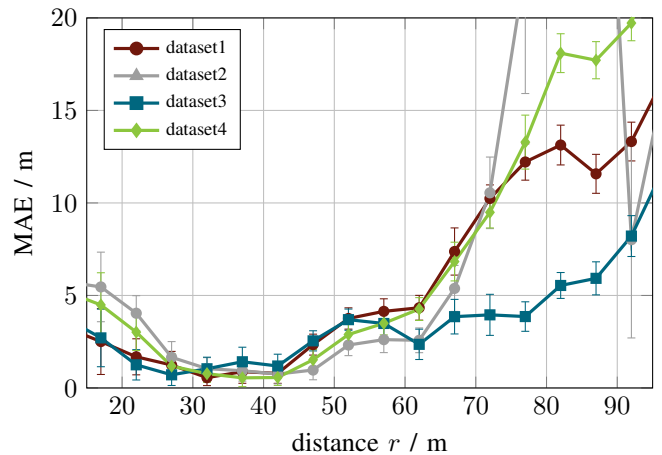


Fig. 10: Mean absolute error (MAE) for different datasets with respect to distance (middle gray target).

IV. EVALUATION

To evaluate our approach, we set up five targets of 175x60 cm with different reflectances, see Fig. 9. The lidar signals of both systems vanish on the targets at approximately 100m. Therefore, we record data for evaluation by slowly driving to the targets, starting from 100m distance and stopping at 10m. As for the training and validation set, pixel intensity triples and a corresponding lidar depth are exported. We can only use three targets (middle gray, dark gray, black) for evaluation because the white and light gray target cause too many saturated pixels in all slices and we obtain too few points for evaluation. In total, 8103 points are obtained for the black target, 4169 for the dark gray target and 2072 for the middle gray target.

A. Dataset Evaluation

At first, our different datasets are compared by considering the MAE with respect to distance. Fig. 10 shows the MAE calculated on distance bins of 5 m. The accuracy of our different datasets is quite similar in between 25–45 m. There exist huge differences for small (< 25 m) and large (> 45 m) distances in particular. dataset2 and dataset4, which contain many noisy points, yield the worst performance for these edge regions. This indicates that noisy training data

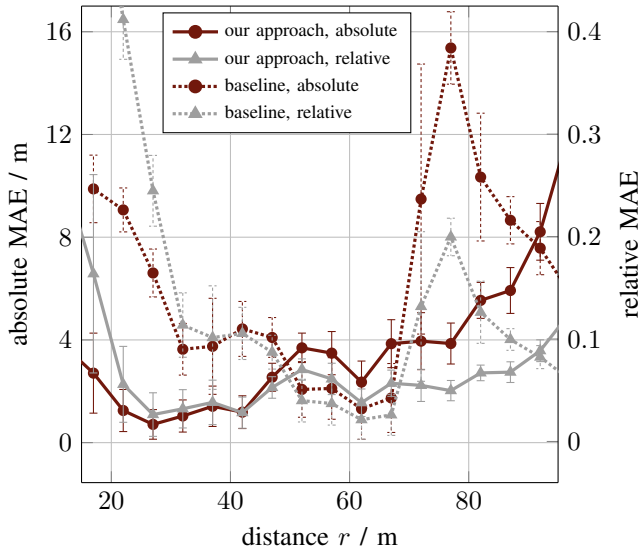


Fig. 11: Absolute and relative mean absolute error (MAE) for our approach and our baseline algorithm.

are bad for approximating the function. It can be clearly seen that the softened filter conditions for large distances in *dataset3* compared to *dataset1* help to improve accuracy at greater distances.

For the further evaluation, we use only the NN trained with the best performing *dataset3*.

B. Baseline Comparison

As depicted in Fig. 11, our baseline algorithm shows best performance between 50–70 m. This is reasonable because in this region all three slices overlap. Our approach trained on *dataset3* outperforms the baseline algorithm in any region except 50–70 m. As Fig. 7 shows, there are quite few training samples for distances larger than 50 m which explains the worse performance. We expect that by collecting more data in this region, the NN performance will beat the baseline. The relative MAE in Fig. 11 shows that for our approach a stable relative accuracy of 5% is achieved in the range between 25–80 m. By design, accuracy is worse for near and far regions because these ranges are covered only by 1-2 slices. The accuracy of the baseline algorithm varies, probably because in some regions the simulated RIPs match the real RIPs better and in other regions worse.

The better performance of our approach suggests that the NN is able to capture the real RIP shapes of the slices whereas the baseline algorithm is limited to the simulated RIPs with rectangular shape assumptions. While our approach is limited by the range of the lidar reference system, the baseline approach can estimate distances for our gated parameters theoretically up to 123 m. Further work should definitely include a baseline approach with more realistic assumptions.

C. Independence Evaluation

Fig. 12 depicts the MAE and the relative MAE for three targets with a different reflectance. Both baseline and NN

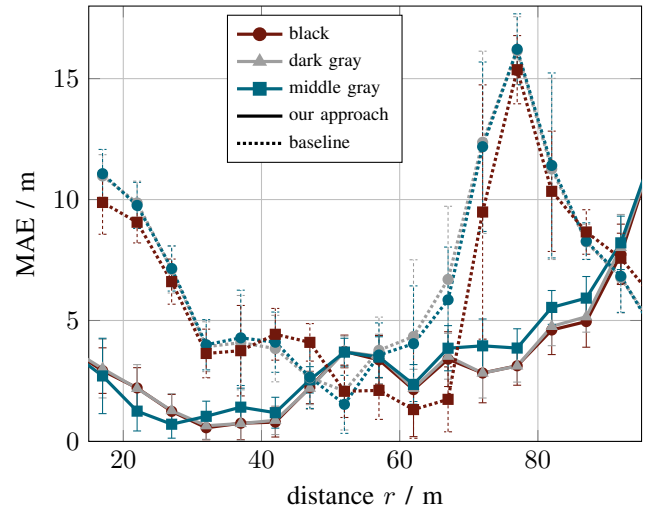


Fig. 12: Mean absolute error (MAE) for different targets (black target, dark gray target, middle gray target).

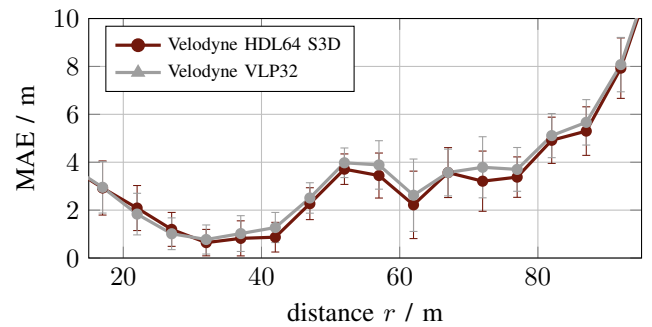


Fig. 13: Mean absolute error (MAE) evaluated for different reference measurement systems.

algorithm show a similar behavior within the error bars for different reflectances. This means that our approach is independent of the reflectance of the targets. However, if the reflectance of the target is too high, it is possible that the corresponding pixel can be saturated in each slice and therefore no depth information can be captured.

In Fig. 13, one can see the MAE taken for two different reference systems. Fig. 13 clearly shows that our reference measurement system can be considered reliable.

D. Which function was learned?

Finally, we will take a close look into which function the NN has learned. Every possible valid intensity triple is fed into our algorithm. An intensity triple is considered as valid if all values are smaller than 250, the difference between maximum and minimum intensity is larger than 6 and the intensity of the middle slice is not the minimum. In total, approximately 8 million combinations are evaluated. Since the algorithm is trained by *dataset3* that consists of a subset of all possible combinations (14223 samples, 0.18% of all 8 million combinations), the NN can be considered as interpolator for intensity triples not included in the training dataset.

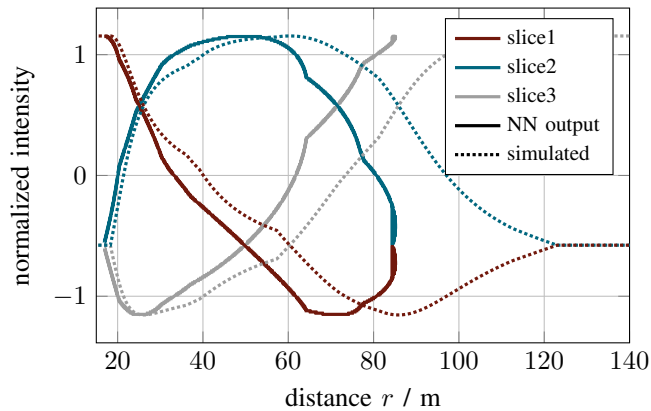


Fig. 14: Learned function illustrated by plotting normalized intensities according to depth. Simulated values are based on the range intensity profiles as depicted in Fig. 5.

Fig. 14 illustrates the normalized intensities of each slice according to the estimated depth. Additionally, the normalized intensities from our simulated RIP based on rectangular assumptions are included for reference. It can be seen that the normalized simulated RIP can be rediscovered in the NN output. Any differences probably come from the fact that in contrast to simulation, NN is able to capture the real RIP. Moreover, Fig. 14 clearly indicates that the NN only learns distances in between 18–85 m. This explains the large errors for the edge regions.

V. CONCLUSION

In this work, we present an approach to estimate distance from active gated image slices by training a NN. This approach is independent from the target reflectance, the reference sensor and the shape of the RIPs. We showed, that the NN is able to learn the shape of the RIPs using training data. Only three slices are required in order to obtain a relative accuracy of 5% for distances between 25–80 m. Thus, a baseline algorithm based on the classical idea of range intensity correlation is outperformed. Thanks to the resolution of the gated camera (1280x720), a super-resolved depth is obtained and by design perfectly aligned to the gated image.

Since active illumination is required, eye-safety restrictions, interference with other systems and shadowing effects have to be handled. In contrast to a lidar system it is not possible to adapt the illumination power pixel wise. If saturated pixels appear, then no depth restoration is possible. A gated camera usually has a significantly better range than automotive lidar systems. However, this approach is limited by the range of the lidar system.

There is great potential for improving many different aspects of the system. Pixel-wise distance estimation is done by an extremely small network with a single hidden layer incorporating 40 nodes with a ReLU activation function. If one intend to adapt the RIP to certain weather conditions, i.e. small range for foggy weather and maximum range for good weather, fine tuning the network on the fly gives

maximum flexibility. By using more and better overlapping slices, accuracy will certainly improve.

ACKNOWLEDGMENT

The research leading to these results has received funding from the European Union under the H2020 ECSEL Programme as part of the DENSE project, contract number 692449.

REFERENCES

- [1] M. Bijelic, T. Gruber, and W. Ritter, "Benchmarking Image Sensors Under Adverse Weather Conditions for Autonomous Driving," in *IEEE Intelligent Vehicle Symposium*, 2018.
- [2] P. Heckman and R. T. Hodgson, "2.7 Underwater Optical Range Gating," *IEEE Journal of Quantum Electronics*, vol. 3, no. 11, pp. 445–448, 1967.
- [3] R. G. Driggers, "Impact of speckle on laser range-gated shortwave infrared imaging system target identification performance," *Optical Engineering*, vol. 42, no. 3, p. 738, 2003.
- [4] S. Inbar and O. David, "Laser gated camera imaging system and method," US Patent US7379164B2, May 27, 2008.
- [5] G. R. Fournier, D. Bonnier, J. L. Forand, and P. W. Pace, "Range-gated underwater laser imaging system," *Optical Engineering*, vol. 32, no. 9, p. 2185, 1993.
- [6] J. Busck and H. Heiselberg, "Gated viewing and high-accuracy three-dimensional laser radar," *Applied Optics*, vol. 43, no. 24, pp. 4705–10, 2004.
- [7] J. Busck, "Underwater 3-D optical imaging with a gated viewing laser radar," *Optical Engineering*, 2005.
- [8] D.-M. He, "Underwater lidar imaging scaled by 22.5 cm/ns with serial targets," *Optical Engineering*, vol. 43, no. 3, p. 754, 2004.
- [9] P. Andersson, "Long-range three-dimensional imaging using range-gated laser radar images," *Optical Engineering*, vol. 45, no. 3, p. 034301, 2006.
- [10] S. Y. Chua, X. Wang, N. Guo, C. S. Tan, T. Y. Chai, and G. L. Seet, "Improving three-dimensional (3D) range gated reconstruction through time-of-flight (TOF) imaging analysis," *Journal of the European Optical Society*, vol. 11, 2016.
- [11] M. Laurenzis, F. Christnacher, and D. Monnin, "Long-range three-dimensional active imaging with superresolution depth mapping," *Optics Letters*, vol. 32, no. 21, pp. 3146–8, 2007.
- [12] M. Laurenzis, F. Christnacher, N. Metzger, E. Bacher, and I. Zielenski, "Three-dimensional range-gated imaging at infrared wavelengths with super-resolution depth mapping," in *SPIE Infrared Technology and Applications XXXV*, vol. 7298, 2009.
- [13] W. Xinwei, L. Youfu, and Z. Yan, "Triangular-range-intensity profile spatial-correlation method for 3D super-resolution range-gated imaging," *Applied Optics*, vol. 52, no. 30, pp. 7399–406, 2013.
- [14] Z. Xiuda, Y. Huimin, and J. Yanbing, "Pulse-shape-free method for long-range three-dimensional active imaging with high linear accuracy," *Optics letters*, vol. 33, no. 11, pp. 1219–1221, 2008.
- [15] C. Jin, X. Sun, Y. Zhao, Y. Zhang, and L. Liu, "Gain-modulated three-dimensional active imaging with depth-independent depth accuracy," *Optics Letters*, vol. 34, no. 22, pp. 3550–3552, 2009.
- [16] B. Göhler and P. Lutzmann, "Super-resolution depth information from a shortwave infrared laser-gated viewing system by using correlated double sampling," *SPIE Electro-Optical Remote Sensing XI*, vol. 10434, p. 22, 2017.
- [17] D. Eigen, C. Puhrsch, and R. Fergus, "Depth Map Prediction from a Single Image using a Multi-Scale Deep Network," in *Advances in Neural Information Processing Systems*, 2014, pp. 2366–2374.
- [18] E. Sonn, A. Oved, E. Levi, Y. Grauer, and O. David, "Gated Imaging, Apparatus, System and Method," WO Patent WO 2017/149370 A1, Sep 8, 2017.
- [19] K. Hornik, M. Stinchcombe, and H. White, "Multilayer feedforward networks are universal approximators," *Neural Networks*, vol. 2, no. 5, pp. 359–366, 1989.
- [20] D. E. Rumelhart, G. E. Hinton, and R. J. Williams, "Parallel Distributed Processing: Explorations in the Microstructure of Cognition, Vol. 1." Cambridge, MA, USA: MIT Press, 1986, pp. 318–362.
- [21] I. Goodfellow, Y. Bengio, and A. Courville, *Deep Learning*. MIT Press, 2016, www.deeplearningbook.org.